Published in final edited form as:
Mol Pharm. 2013 May 6; 10(5): 2031–2044. doi:10.1021/mp400054e.

Biodistribution and Pharmacokinetics of EGFR-Targeted Thiolated Gelatin Nanoparticles Following Systemic Administration in Pancreatic Tumor-Bearing Mice

Jing Xu[†], **Florence Gattacceca**[†,§], and **Mansoor Amiji**[*,†]

[†]Department of Pharmaceutical Sciences, School of Pharmacy, Northeastern University, Boston, MA, United States

[§]Department of Pharmacokinetics, EA4215, Faculté de Pharmacie, Université Montpellier 1, 15 av. Ch. Flahault, 34093 Montpellier Cedex 5, France

Abstract

The objective of this study was to evaluate qualitative and quantitative biodistribution of epidermal growth factor receptor (EGFR)-targeted thiolated type B gelatin nanoparticles *in vivo* in a subcutaneous human pancreatic adenocarcinoma (Panc-1) bearing female SCID Beige mice. EGFR-targeted nanoparticles showed preferential and sustained accumulation in the tumor mass, especially at early time points. Higher blood concentrations and higher tumor accumulations were observed with PEG-modified and EGFR-targeted nanoparticles during the study (AUC_{last}: 17.38 and 19.56 %ID/mL*h in blood, 187 and 322 %ID/g*h in tumor for PEG-modified and EGFR-targeted nanoparticles, respectively), as compared to control, unmodified particles (AUC_{last}: 10.71 %ID/mL*h in blood and 138 %ID/g*h in tumor). EGFR-targeted nanoparticles displayed almost twice tumor targeting efficiency than either PEG-modified or the unmodified nanoparticles, highlighting the efficacy of the active targeting strategy. In conclusion, this study shows that EGFR-targeted and PEG-modified nanoparticles were suitable vehicles for specific systemic delivery in subcutaneous Panc-1 tumor xenograft models.

Keywords

Thiolated type B gelatin nanoparticles; poly(ethylene glycol); epidermal growth factor receptor (EGFR) targeting; long circulation time; passive tumor targeting; active tumor targeting; biodistribution; targeting efficiency; pharmacokinetics; two compartment model; population analysis

1. INTRODUCTION

A major obstacle in cancer therapy is targeted delivery of therapeutic agents to specific disease sites in the body. One of the strategies to address this problem is focused on novel development of tumor specific nanomedicines.[1] Applications of liposomes, micelles, and polymeric nanoparticles have shown to improve delivery of small molecule drugs and genetic materials to selective targets, including intracellular accumulation in specific subcellular organelles.[2-4] To accomplish and continue to improve on this goal, the delivery vectors need to recognize the host cells, avoid nonspecific binding and uptake, resist degradation during the systemic circulation and after reaching the target cells, they should

[*]***Corresponding author:*** Mailing Address: Department of Pharmaceutical Sciences, School of Pharmacy, Northeastern University, 360 Huntington Ave, Boston, MA 02115 Tel. (617) 373-3137 Fax (617) 373-8886 m.amiji@neu.edu.

cross the cell membrane, afford escape from endosomal/lysosomal compartment, release genes from the complex and let the cargo get into the nucleus or accomplish its function in the cytoplasm (e.g., for small interfering RNA).[5] For targeted delivery to solid tumors *in vivo*, nanoparticles can accumulate at the site either by passive or active mechanisms.[1]

Due to rapid proliferation and growth during tumor progression, solid tumors are characterized by heterogeneous vasculature, which has big gap junctions between endothelial cells and lack of lymphatic drainage.[6] Nanovectors with diameter around 200 nm and hydrophilic surface, such as the poly(ethylene glycol) (PEG) modified, have been proven to remain in the blood stream for a longer duration and they are also able to reach the tumor mass through extravasation at higher concentrations.[7] The pathophysiologic feature of these types of nanovectors is termed the "enhanced permeability and retention" (EPR) effect, and Maeda *et al*.[8] have firstly proven this effect in preclinical models with polymer-conjugated anticancer therapeutics. Based on the EPR effect, polymeric nanoparticles can be surface-modified with hydrophilic polymer chains to achieve targeting. PEG or poly(ethylene oxide) (PEO), with a structure of HO-$(CH_2CH_2O)_n$-CH_2CH_2-OH is a common polymer that has been used for this purpose.[9] Modification with these polymers could form dense hydrophilic shell of long chains and protect the nanoparticles from interacting with different solutes, especially on physiologic level, achieving steric stabilization to prevent non-specific hydrophobic interaction with the reticulo-endothelial system (RES), protein binding and complement activation.[9] Meanwhile, during proliferation, cancer cells usually present higher metabolic rate and express different levels of enzymes and proteins, such as redox enzymes and glutathione.[10, 11] Design of a polymeric system with disulfide crosslinks could trigger glutathione-induced intracellular delivery of the encapsulated payload in cancer cells.[12]

With passive targeting, most cancer therapy vectors still have intrinsic limitation, lack of specificity. Thus, modification of delivery system with targeting moieties could achieve the second strategy: active targeting. In this strategy, unique properties of cell surface will need to be identified initially to differentiate target cells population with normal cells.[1] Depending on the levels of receptors or antigens on the target cells, substrate or antibodies could be conjugated on delivery system, and assist the system to target specifically. Ideally, after interaction between targeting moiety and cell marker, internalization and endocytosis process could be triggered.[7]

Research has shown that more than 80% pancreatic cancer patients have advanced stage disease with metastasis to liver, spleen, and the gastro-intestinal tract at the time of diagnosis, and EGFR expression is a very important marker of disease aggression and dissemination.[13] Previous studies with genetically modified mice model of pancreatic cancer have shown that EGF receptor signaling pathway was a critical factor for regulating pancreatic epithelial differentiation and initiating pancreatic tumorigenesis.[14, 15] Thus, amplification of EGF receptor expression was observed since the initiation of pancreatic intraepithelial neoplasia (PanIN).[16] Results in laboratory and clinical research have shown that expression of EGFR closely relate to tumor invasiveness and resistance to therapy.[17-21] Based on this, our system is designed to systemically deliver therapeutic agents in the gelatin nanoparticles conjugated with EGFR-targeted peptide. The synthetic 12 amino acids peptide GE11 with the sequence NH_2.Y-H-W-Y-G-Y-T-P-Q-N-V-I-CO_2H has been shown to target EGFR receptor *in vitro* and *in vivo*.[22-26] Previous studies have also shown that this peptide could induce cellular uptake of nanoparticles without induction of EGFR-specific mitogenic and stimulatory activity.[26] By modification with hetero-functional PEG, the peptide would anchor on the surface and remain sufficiently flexible for efficient receptor binding.[27]

To combine the two strategies in the same system, type B gelatin was chosen for preparation of the engineered nanocarriers. Gelatin is one of the most versatile natural biopolymers derived from collagen, and it has been widely used in food products and medicines.[28, 29] As a biodegradable, non-toxic, and non-immunogenic material, gelatin serves a variety of functions in products administered into the systemic circulation including use as a stabilizer in protein formulations[30, 31], gels for in situ tissue engineering[32, 33], microspheres for therapeutic embolization[34, 35], and sponges to prevent post-surgical adhesions.[36] With solvent displacement, type B gelatin, derived from alkaline hydrolysis of collagen, could wrap up and form nanoparticles.[37, 38] Free amino acids groups on gelatin also provide the possibility for further modification. With addition of sulfhydryl groups, thiolated gelatin could serve as a biocompatible, biodegradable, and non-condensing polymeric matrix for delivery of therapeutic agents.[39, 40] Further modification with PEG and targeting peptide on the surface of thiolated gelatin nanoparticles can lead to efficient and specific accumulation at the tumor site and internalization in cells.[41, 42]

In a previous study, we have described the synthesis of thiolated gelatin using type B gelatin and 2-iminothiolane, preparation of EGFR targeted thiolated gelatin nanoparticles, and cytosolic DNA delivery potential in response to higher intracellular glutathione concentrations.[39-45] Cell trafficking studies showed rapid uptake and plasmid release of EGFR-targeted nanoparticles in Panc-1 pancreatic adenocarcinoma cells. Qualitative and quantitative analysis of transfection in Panc-1 cells by nanoparticles carrying plasmid DNA encoding for enhanced green fluorescent protein (EGFP-N1) and tumor suppressor protein (p53) was performed by fluorescence microscopy, ELISA and RT-PCR. Delivery of reporter plasmid with EGFR-targeted nanoparticles resulted in highest levels of GFP expression relative to other controls, including Lipofectin, a commercially available cationic lipid transfection reagent, especially at 48 h post transfection. With the same system, transfection with wild-type p53 (wt-p53) protein induced rapid apoptosis process in Panc-1 cells.[41] The high transfection efficiency associated with EGFR targeted thiolated gelatin nanoparticles could be attributed to the active targeting of EGFR receptor of Panc-1 cells, increased stability from additional disulfide crosslinking, triggering release of the payload in a intracellular reducing environment, noncomplexed DNA delivery system, and reduced cytotoxicity. These results suggest that the EGFR-targeted thiolated gelatin nanoparticles can serve as safe and efficient DNA delivery system for gene therapy as a treatment for pancreatic cancer.

In this study, we have investigated the biodistribution and tumor-targeting potential of the unmodified (SH-Gel NP), PEG-modified (SH-Gel PEG) and EGFR targeting peptide conjugated (SH-Gel PEG Peptide) thiolated gelatin nanoparticles *in vivo* in human pancreatic carcinoma (Panc-1)-bearing SCID beige mice. Non-compartmental and population compartmental pharmacokinetic analysis was performed to compare the distribution parameters among different nanoparticles treatments.

2. MATERIALS AND METHODS

2.1 Materials

Type B gelatin (225 bloom strength), crosslinking reagent Glyoxal (40% v/v), Indocyanine green (ICG) and diethylenetriaminepentaacetic acid were purchased from Sigma-Aldrich (St. Louis, MO). Methoxy-PEG-succinimidylcarboxymethyl ester (mPEG-SCM, MW 2,000 Da) was purchased from Laysan Bio Inc. (Arab, AL). Maleimide-PEG-*N*-hydroxysuccinimide ester (MAL-PEG-NHS, MW 2,000 Da) was purchased from JenKem (Allen, TX). EGFR specific peptide was synthesized at Tufts University's Peptide Synthesis Core Facility (Boston, MA). Methanol, chloroform, dimethylsulfoxide and absolute ethyl alcohol (200 proof, 99-5% ACS reagent) were obtained from Acros Chemicals (Pittsburgh,

PA). Panc-1 human pancreatic adenocarcinoma cell line was purchased from the American Type Culture Collection (ATCC, Manassas, VA). Indium-111 Chloride was purchased from Perkin Elmer (Waltham, MA). BD Matrigel™ Basement Membrane Matrix HC was purchased from BD Biosciences (San Jose, CA). HyClone WFI Quality Water was purchased from Thermo Scientific (Billerica, MA). For anesthesia, IsoSol vapor was purchased from Vedco (St. Joseph, MO).

2.2 Synthesis of Thiolated Gelatin Nanoparticles

Thiolated type B gelatin was synthesized as reported previously.[40, 41] It was prepared by covalent modification of the primary amino groups of type-B gelatin by the addition of sulfahydryl moieties. For the synthesis, 1 g of gelatin was dissolved in 100 mL of deionized water at 37°C and then incubated with 20mg of 2-iminothiolane hydrochloride at room temperature overnight. Any unreacted 2-iminothiolane was removed by repeated dialysis against 5 mM HCl for twice, followed by 1 mM HCl solution for 3 h each. The purified thiolated gelatin was dried in vacuo and stored at 4°C for further use.

Based on initial cytotoxicity and transfection results[41], the nanoparticles for these studies were prepared with thiolated gelatin. The nanoparticles were prepared as previous reported.[41] 200 mg thiolated gelatin was dissolved in water and pH of solution was adjusted to 7-0 by addition of 0-2 M NaOH solution. For ICG encapsulation, 10 mg ICG was added and gently mixed with thiolated gelatin solution. Chilled ethanol was added slowly into the mixture while stirring solution at high speed. Nanoparticles were formed when solvent composition changed to 75% hydro-alcoholic solution. Nanoparticles were further crosslinked by slow addition of 0.1 mL of 8% (v/v) glyoxal solution. Unreacted reagents were quenched with 0.5 mL of 0.2 M glycine solution. Nanoparticles were ultra-centrifuged at 16,000 rpm for 30 minutes. Pellets were washed with deionized water twice and purified nanoparticles were freeze-dried and stored at 4°C.

2.3 Surface Modification with EGFR Targeting Peptide

PEG-modified nanoparticles and EGFR targeted nanoparticles were synthesized as described previously.[39, 41, 42] Nanoparticles were re-suspended in 0.1 M phosphate buffer (pH 7.4) with concentration of 10 mg/mL and incubated with 2 times weight of methoxy-PEG-succinimidylcarboxy methyl ester (mPEG-SCM, MW 2,000 Da) or maleimide-PEG-succinimidylcarboxy methyl ester (MAL-PEG-SCM, MW 2,000 Da) for 2 hours at room temperature with slow stirring. PEG-modified nanoparticles were collected with ultra-centrifugation at 16,000 rpm for 30 minutes. Pellets were washed with deionized water twice and purified nanoparticles were freeze-dried and stored at 4°C. MAL-PEG-SCM modified nanoparticles were suspended in 0.1M phosphate buffer (pH 6.5) with concentration of 10 mg/mL and incubated with 10% weight of EGFR specific peptide with 4 glycine residues as spacer and a terminal cysteine (i.e., Y-H-W-Y-G-Y-T-P-Q-N-V-I-*G-G-G-G-**C***) for 6 hours at room temperature with slow stirring. The sulfhydryl group of cysteine will react with the maleimide functionality of the PEG. Peptide modified nanoparticles were then collected with ultra-centrifugation at 16,000 rpm for 30 minutes. Pellets were washed with deionized water twice and purified nanoparticles were freeze-dried and stored at 4°C. Fluorescein isothiocyanate (FITC) labeled peptides were conjugated to the nanoparticles instead for quantitative determination of peptide conjugation.

2.4 Characterization of Control and Targeted Nanoparticles

As described previously, for characterization of nanoparticles, they were suspended in water at a concentration of 1 mg/mL. Suspension was analyzed using Zetasizer Nano (Malvern Inc).[41] Particle size analysis was carried out at a scattering angle of 90 degrees at 25°C. Zeta potential was measured at default parameters of dielectric constant, refractive index and

viscosity of water at 25°C. Lyophilized nanoparticles were mounted on aluminum sample mount and sputter-coated with palladium to enhance conductivity and minimize buildup of charges. Samples were observed for surface morphology under a Hitachi 4800 field emission scanning electron microscope at 3 kV. For FITC conjugated peptide, after synthesis, peptide conjugated nanoparticles suspensions were measured for fluorescence intensity with BioTek Synergy HT plate reader with excitation at 490 nm and emission at 525 nm. FITC-peptide solution was used for standard curve. For ICG encapsulated nanoparticles, after synthesis, nanoparticles suspensions were measured with BioTek Synergy HT plate reader for absorbance at 790 nm. Concentrations of ICG and encapsulation ratios were calculated based on the standard curve.

2.5 Radiolabeling with ^{111}Indium

In order to determine the fate of the nanoparticles in various tissues in the body after intravenous administration, radionucleide indium-111 chloride ($^{111}InCl_3$) was used for labeling unmodified (SH-Gel NP), PEG modified (SH-Gel PEG) and EGFR targeted (SH-Gel PEG Peptide) thiolated gelatin nanoparticles. With half-life of 68 hours at 171 keV, 245 keV gamma rays and absence of beta-emission, ^{111}In could serve as an excellent molecule for radioactivity applications, especially for *in vivo* studies. Molecules of indium could be attached to gelatin nanoparticles systems through a bifunctional chelator, diethylenetriaminepentaacetic acid (DTPA). For DTPA conjugation, nanoparticles were synthesized and suspended at a concentration of 5 mg/mL in 1M HEPES buffered saline (HBS, pH 7.5). To nanoparticles suspension, anhydride DTPA (4 mg/mL), dissolved in dimethylsulfoxide, was added under constant stirring at room temperature. During this process, free amino groups remaining after surface modification were used to couple cyclic anhydride DTPA. The nanocarrier–DTPA mixture was incubated at room temperature for 1 hour and the excess DTPA could be removed by centrifugation at 16,000 rpm for 30 min. The nanoparticles were washed and centrifuged twice to ensure proper removal of free DTPA. DTPA-nanoparticles were then suspended in DI water, followed by addition of 1 mCi $^{111}InCl_3$ solution. After reaction between nanoparticles suspension and $^{111}InCl_3$ for 1 hour at room temperature, nanoparticles were ultra-centrifuged at 16,000 rpm for 30 min to remove free radioactivity. The radiolabeled nanoparticles were re-suspended and centrifuged repeatedly, and the supernatant was measured for any traces of free radioactivity using Cobra® II Auto-Gamma counter (Perkin Elmer, Waltham, MA). The nanoparticles were considered stably labeled with ^{111}In, when the radioactivity in the supernatant reached a minimal value. The radiolabeled nanoparticles were then resuspended in water for measurement of radioactivity. Conjugation ratio of ^{111}In was determined by the radioactivity of nanoparticles divided by the amount added to the reaction. The specific radioactivity in SCi/mg of nanoparticles was then assessed, in order to estimate the amount of radiolabeled nanoparticles to be injected per animal.

2.6 *In Vivo* Biodistribution and Pharmacokinetic Analyses

2.6.1 Panc-1 Cell Culture Conditions—Panc-1 pancreatic adenocarcinoma cell line derived from pancreatic epitheloid carcinoma of a Caucasian male was obtained from ATCC and used for developing tumors in SCID Beige mice. Cells were grown as a monolayer in culture using DMEM supplemented with L-glutamine, 1% Pen-strep and 10% fetal bovine serum at 37°C and 5% CO2.

2.6.2 Animal Model Development—All *in vivo* experiment procedures have been approved by Northeastern University's Institutional Animal Care and Use Committee as well as Radiation Safety Committee within Office of the Environmental Health and Safety. Six weeks old female SCID Beige mice, weighing approximately 20 g, were purchased from Charles River Laboratories (Wilmington, MA) and were used for the biodistribution study.

Upon arrival, the animals were group-housed in the Division of Laboratory Animal Medicine at Northeastern University and supplied with sterile rodent pellets and water *ad libitum*. The animals were allowed to acclimate for at least 48 h prior to any experimentation.

To inoculate subcutaneous tumors, animals were mildly anesthetized by inhalation of 2% IsoSol vapor (St. Joseph, MO) in 100% oxygen and approximately 3 million Panc-1 cells in 200 SL of phosphate buffered saline (PBS) and Matrigel mixture were injected subcutaneously into the left flanks of female SCID Beige mice. Tumor volume was monitored by measuring tumor size with caliper every 3 days. Tumor volume (in mm^3) was then calculated using this formula: $Volume=0.52\times Length\times Width^2$. Three to four weeks were allotted for the tumors to grow and reach a palpable volume and during this period, the animals were monitored daily for food/water intake, body weight and any physical signs of discomfort. Any animals that seemed lethargic were sacrificed.

2.6.3 Qualitative Biodistribution Studies—Four different samples were prepared: ICG encapsulated unmodified (SH-Gel NP), PEG modified (SH-Gel PEG) and EGFR targeted thiolated gelatin nanoparticles (SH-Gel PEG Peptide) suspensions, and a 10^{-4} M solution of free ICG in WFI Quality Water. 200 SL of nanoparticles suspension containing 16 Sg of ICG or free ICG dye were intravenously injected into female SCID beige mice bearing Panc-1 human pancreatic adenocarcinoma xenograft, whose size was around 500 mm^3. Near-infrared transillumination images were recorded using an *In Vivo* FX whole animal imaging station (Rochester, NY). The animals were placed into the imaging chamber, and anesthesia was induced and maintained by inhalation of 2% IsoSol vapor (isoflurane; Vedco, St. Joseph, MO) in 100% oxygen. Each mouse was positioned laterally on its left side for imaging. A 3 min exposure was recorded under NIR excitation using a 720 and 750 nm bandpass excitation and emission filter set, respectively. Next, an X-ray image (10 s exposure at 35mV) was recorded of the mice in the same position to be used as an underlying reference. The separate NIR fluorescence and X-ray images were then merged to illustrate signal distribution relative to anatomy. This anesthesia and imaging procedure was repeated for each time point (1, 2, 4, 6 and 12 hours) over a period of 12 hours. The NIR images were pseudo-colored and merged with the underlying X-ray images using Carestream (Kodak) imaging software (Rochester, NY). The imaging studies were conducted on 8 mice for a total of 4 separate study groups.

2.6.4 Quantitative Biodistribution Studies—For quantitative biodistribution study, three different samples were prepared: ^{111}In labeled unmodified (SH-Gel NP), PEG modified (SH-Gel PEG) and EGFR targeted thiolated gelatin nanoparticles (SH-Gel PEG Peptide) suspensions in WFI Quality Water. After tumor volume reached 150 mm^3, 72 tumor-bearing mice were divided to 3 groups for different formulations, 4 mice were used at every time points, 6 time points were assessed per set. Panc-1 Pancreatic adenocarcinoma bearing mice were injected intravenously via the tail vein with 200 SL nanoparticles suspension with equivalent to 2 SCi dose of ^{111}In radioactivity. The mice were sacrificed by cervical dislocation following anesthetization at specific time points of 0.25, 1, 2, 6, 12 and 24 hours after administration. Blood, tumor, and highly perfused organs such as heart, liver, kidneys, spleen, and lungs as well as pancreas and muscle were excised. Weight of each organ was recorded and corresponding radioactivity in that organ recorded with gamma counter. The number of counts per minute (CPM values from gamma counter) was converted to disintegrations per minute (DPM) by dividing radioisotope efficiency (94% for ^{111}In). Percentage activity was calculated with DPM divided by injected radioactivity. Percentage dose per gram of tissue or fluid was calculated with percentage activity divided by weight of tissue. The concentration of nanoparticles in blood, tumor, and other tissues was expressed as percent of recovered dose per milliliter of blood or per gram of tissue.

2.6.5 Pharmacokinetic Analysis—Pharmacokinetic parameters were calculated taking into account all individual data, using Phoenix® WinNonlin® v. 1.3 software (Pharsight, Cary, NC, USA). A non-compartmental analysis (NCA) was performed for all organs and tissues. The slope of the terminal log-linear part of the concentration versus time curve (Lambda_z) was calculated using the best-fit method, weighting the data in $1/y^2$. A population analysis using FO algorithm was also performed to calculate additional pharmacokinetic parameters from blood data. The parameters were assumed to be log-normally-distributed. The population model was chosen based on Bayesian Information Criterion (BIC) and goodness of fit plots. The two-compartmental structural model with an additive error model best fitted the data. The model was parameterized in V_1, K_e, K_{12} and K_{21}, ie microconstants parameterization. Secondary population parameters were calculated by the Phoenix® WinNonlin® software based on the following equations: $CL = V_1*K_e$; $AUC_{inf} = Dose/CL$; $V_2 = K_{12}/K_{21}*V_1$; $V_{ss} = V_1+V_2$; $MRT = V_{ss}/CL$; $Beta = 0.5*(K_{12}+K_{21}+K_e - sqrt((K_{12}+K_{21}+K_e)*exp(2) - 4*K_{21}*K_e)$; $Alpha = K_{21}*K_e/Beta$; $A = 1/V_1*(Alpha - K_{21})/(Alpha - Beta)$; $B = 1/V_1*(Beta - K_{21})/(Beta - Alpha)$; $HL\ rate = 0.693/rate$. Graph Pad Prism software (GraphPad Software, La Jolla, CA, USA) was used for statistical analysis. The two-tailed unpaired homoscedastic t-test was used to compare mean values ± standard errors: p values < 0.05 were considered statistically significant.

3. RESULTS

3.1 Synthesis of EGFR-Targeted Nanoparticles

With reaction between 2-iminothiolane and gelatin, thiolated gelatin contains 6.08 mmol/g sulfhydryl groups as previously determined.[40] Since isoelectric point of gelatin is around 4.5-5.5, after adjustment of the pH of thiolated gelatin solution to 7, gelatin nanoparticles presented negative charges. The initial free amino groups on the surface of gelatin and thiolated gelatin nanoparticles were considered as 100%. Upon incubation with excess methoxy-PEG-succinimidylcarboxy methyl ester (mPEG-SCM) or maleimide-PEG-succinimidylcarboxy methyl ester (MAL-PEG-SCM), which has functional group succinimidylcarboxy methyl ester specifically reacting with amine groups, surface amino groups of thiolated nanoparticles were largely decreased as proven in previous studies.[39] With 2 hours incubation, about 90% of the surface-accessible amine groups were modified upon incubation with two times molar excess of PEG-succinimidylcarboxy methyl ester. EGFR specific peptide (Y-H-W-Y-G-Y-T-P-Q-N-V-I-*G-G-G-G-C*) was further conjugated to the terminal of PEG through a nucleophilic addition reaction between maleimide groups of hetero-bifunctional PEG and the cysteine sulfhydryl groups of the peptides.

3.2 Characterization of Control and EGFR Peptide-Modified Nanoparticles

The nanoparticles prepared by desolvation were characterized for particle size and zeta potential. The mean particle diameters of different nanoparticles were between 150-250 nm. For SH-Gel NP, the average size was found to be in the range of 132.6 ± 17.9 nm. With different surface modifications, sizes of nanoparticles have changed. SH-Gel PEG was found to have a larger particle size, 179.0 ± 30.9 nm, while SH-Gel PEG Peptide had particle size around 230.8 ± 41.5 nm. The increase in size of the nanoparticles clearly indicates the addition of PEG and peptide molecules on the surface of the nanoparticles, which results in the change in hydrodynamic diameter of the system in aqueous environment. Even with peptide conjugation, the nanoparticles will still have the size range below 250 nm that is necessary for accumulation in solid tumor by the EPR effect. SH-Gel NP had zeta potential of −24.6 ± 5.16 mV. In comparison, SH-Gel PEG and SH-Gel PEG Peptide were found to have zeta potential of −22.3 ± 9.50 mV and −18.1 ± 4.02 mV, respectively. The slight decrease in the negative charge on the surface of SH-Gel PEG and SH-Gel PEG Peptide could be due to the modification of the surface amino groups.

Scanning electron microscopy (SEM) images in Figure 1 have shown that different thiolated gelatin nanoparticles had spherical shape, smooth surface morphology and sizes of nanoparticles were observed were consistent with Zetasizer results.

High-resolution C1S scans of electron spectroscopy for chemical analysis (ESCA) was previously used to analyze surface component of nanoparticles and has further confirmed PEG and peptide surface modification. Peak intensities of ether linkage signal has increased after PEG modification and decreased after peptide conjugation.[41] Nitrogen composition has decreased after PEG modification and increased after peptide modification, which could further confirm the presence of EGFR-targeting peptide on the nanoparticles. [41] Based on fluorescence intensity of FITC conjugated peptides, it has shown that around 21.7% peptides were conjugated on the surface of nanoparticles. With these quantitative and qualitative analyses, we could confirm the conjugation of EGFR targeted peptides on the surface of nanoparticles.

3.3 *In Vivo* Qualitative Biodistribution Studies

For qualitative biodistribution study, a near IR dye indocyanine green (ICG) was encapsulated into nanoparticles. After synthesis, concentration of ICG in nanoparticles was measured and all types of nanoparticles have encapsulation ratio around 24.3%. Images of mice were overlaid and compared among different formulations as shown in Figure 2. Qualitative biodistribution images revealed that free ICG accumulation couldn't be observed in tumors of mice throughout 12 hours study. However, the mice subjected to different nanoparticle treatment retain their tumor accumulation signal beyond 6 h, and for SH-Gel PEG and SH-Gel PEG Peptide, the signal in tumors can retain visibility even at 12 h. Based on the images, both SH-Gel PEG and SH-Gel PEG Peptide showed quick uptake at 1 h in tumor and sustainable accumulation up to 12 h compared to SH-Gel NP, and SH-Gel PEG Peptide have shown stronger signal compared to SH-Gel PEG at 1 h. Although it's hard to differentiate the amount accumulated for lateral view, based on the images, SH-Gel PEG Peptide have preferential accumulation in tumor compared to liver for up to 4 hours, while SH-Gel PEG showed delayed accumulation in liver since 2 hours. This result further suggests that the nanoparticles are retained in the circulation for prolonged periods of time, and SH-Gel PEG, SH-Gel PEG Peptide preferentially accumulated in tumor.

3.4 Pharmacokinetic Analysis in Blood and Tumor

Nanoparticles were efficiently labeled with ^{111}In with conjugation ratio around 10% (data not shown). After administration of radiolabeled nanoparticles, four mice were sacrificed at each time point. Mean concentrations ± standard deviations (SD) versus time profile of the SH-Gel NP, SH-Gel PEG, and SH-Gel PEG Peptide nanoparticles in blood and tumor, obtained by plotting percentage of recovered radioactivity per gram or mL of samples, as a function of time, are represented in Figure 3. The blood concentration-time profiles of the radiolabeled nanoparticles indicate overall higher concentrations of SH-Gel PEG and SH-Gel PEG Peptide as shown in Figure 3A, when compared to SH-Gel NP.

A non-compartmental analysis (NCA) and a population analysis of all individual blood data were performed and allowed the calculation of pharmacokinetic parameters (Table 1). As shown by NCA results, blood concentrations were significantly higher for SH-Gel PEG ($p = 0.0071$) and SH-Gel PEG Peptide ($p = 0.0008$), when compared to SH-Gel NP, with AUC ±SE from 0 to 24h (AUC_{last}) being 17.38 (± 1.32), 19.56 (± 1.01) and 10.71 (± 1.01) h* %ID/mL respectively. AUC extrapolated to infinity (AUC_{inf}) followed the same trend, but to a lesser extent, which means that the extrapolated part was higher for SH-Gel NP, due to a smaller Lambda_z, suggesting that the SH-Gel NP nanoparticle would stay longer in the organism. Accordingly, MRT was found to be higher for SH-Gel NP than both SH-Gel PEG

and SH-Gel PEG peptide (32.3 h vs 21.8 h and 15.3 h respectively). Smaller AUC and higher MRT could be explained by a higher non-specific tissue affinity, leading to a higher volume of distribution and smaller blood concentrations. Accordingly, steady-state volume of distribution (V_{ss}) was much higher for SH-Gel NP (173.5 mL) than for SH-Gel PEG (88.2 mL) and SH-Gel PEG Peptide (60.6 mL).

These results were confirmed using a population approach, based on the FO algorithm (Table 1). The best model was a two-compartment model with additive error. The model could hardly evaluate inter-individual variability (ω) and residual error (σ), due to the sparseness of the data, with only one point per animal (data not shown). However, population pharmacokinetic parameters were evaluated with acceptable standard errors, and were validated by bootstrap approach. The model was also found stable using the Profile Module, with ±20% perturbation on every parameter. Covariate testing suggested that the nanoparticle type would significantly influence the K_{21} parameter only. Moreover, no significant difference was observed between SH-Gel PEG and SH-Gel PEG Peptide, which consequently display the same population pharmacokinetic parameters. K_{21} was found to be the limiting factor of the kinetics, as being the lowest rate constant. K_{21} was significantly enhanced by PEG modification, leading to lower V_2 and lower V_{ss} for SH-Gel PEG and SH-Gel PEG Peptide. This finding suggested that SH-Gel PEG and SH-Gel PEG Peptide would remain less long in the peripheral compartment, which could be ascribed to less non-specific affinity to most of the tissues in the organism. Accordingly, and similarly to the NCA results, MRT, half-life of the log-linear terminal part of the curve, and V_{ss} were higher for SH-Gel NP.

Upon modification with PEG and peptide, the ^{111}In-labeled nanoparticles induced in a greater exposure to tumors, as seen in tumor concentration versus time profile in Figure 3B. At 2 h, about 23.2%ID/g tissue was recovered from SH-Gel PEG Peptide nanoparticles group, in contrast to SH-Gel NP and SH-Gel PEG that had 7.7 and 6.4% retention, respectively. At 12 h time point, about 10.3 and 8.4 %ID/g tissue from SH-Gel PEG Peptide and SH-Gel PEG nanoparticles were retained in the tumor, while SH-Gel NP nanoparticles had only 4.5% retention.

3.5 Tissue Biodistribution Studies

Mean concentrations ± standard deviations (SD) versus time profile of the SH-Gel NP, SH-Gel PEG, and SH-Gel PEG Peptide nanoparticles in different organs, obtained by plotting percentage of recovered radioactivity per gram of samples, as a function of time, are represented in Figure 4 for up to 24 h. Throughout the study, a major fraction of the dose was found in the liver. Other than liver, the nanoparticles were predominantly found in the kidneys and spleen and, to a lesser extent, in the lungs.

Calculation of the slope of the terminal log-linear phase was not always possible in organs and tissues, since the decrease of the concentrations in some organs or tissues had barely started. We hence based our interpretation on AUC_{last} as a reflection of exposure (Figure 5A), and on the C_{last}/C_{max} ratio as a reflection of the rate of concentration decline (Table 2). AUC_{last} was evaluated for all organs where concentrations had been measured, using Phoenix® WinNonlin® NCA.

In the organs in which the nanoparticles highly concentrated (liver, kidney and spleen), the only significant difference of exposure was in spleen, with PEG-modified nanoparticles leading to significantly higher spleen exposure than non-PEG-modified nanoparticles. Other organs had low exposure, heart and muscle AUC_{last} being similar to blood AUC_{last}, while lung and pancreas displayed slightly higher AUC_{last}. The C_{last}/C_{max} ratio was the highest for SH-Gel NP in most organs and tissues (blood, heart, kidney, liver, pancreas and spleen),

suggesting that SH-Gel NP nanoparticles would remain longer in these organs and tissues, and consequently in the organism, due to high non-specific affinity to these organs. Strikingly, for kidney, pancreas, spleen, the C_{last} was equal to C_{max} for SH-Gel NP, clearly showing that the decline of concentrations in these organs had not started yet. These results could explain the smaller K_{21} found for SH-Gel NP using the population compartmental analysis.

Targeted nanoparticles induced a significantly higher exposure to tumor tissue, with AUC_{last} being significantly higher for SH-Gel PEG Peptide than for both SH-Gel NP ($p = 0.0002$) and SH-Gel PEG ($p = 0.0030$). The difference between SH-Gel PEG and SH-Gel NP was not significant. Tumor was the only tissue where exposure was significantly different between SH-Gel PEG Peptide and SH-Gel PEG ($p=0.003$), underlining the targeting effect of the Peptide. Moreover, the only tissue where SH-Gel PEG Peptide displayed the highest C_{last}/C_{max} ratio was the tumor, indicating an increased affinity for this tissue leading to a slower decline in concentrations in the tumor. Although not significantly, SH-Gel PEG still displayed a higher tumor exposure and a higher C_{last}/C_{max} ratio than SH-Gel NP, suggesting the possibility of a slight targeting effect of the PEG modification itself. From these results, SH-Gel PEG Peptide seemed to have a higher affinity for the tumor tissue, leading to higher concentrations and slower decrease of the concentrations in the tumor.

However, the enhanced exposure of the tumor to SH-Gel PEG Peptide may not reflect a higher affinity for the tumor, but be simply correlated to a higher blood exposure since AUC_{last} was higher in both tumor and blood. To test this hypothesis, we calculated a new parameter named Targeting Efficiency (TE), which was calculated by Phoenix® WinNonlin® software as the AUC_{last} of the ratio: Ctumor/Cnon-targeted tissue. To compare TE between PEG-modified and non-PEG-modified nanoparticles, a relative targeting efficiency (RTE) was calculated as the ratio: $TE_{PEGylated}/TE_{NP}$. The results are presented for all tissues and organs, as well as for all the non-targeted organs pooled together (Figure 5B).

SH-Gel PEG displayed similar TE as SH-Gel NP, except in pancreas where it was significantly higher due to higher tumor exposure and in spleen where it was significantly lower, due to higher spleen exposure. On the contrary, SH-Gel PEG Peptide, when compared to SH-Gel NP, displayed a significantly higher TE in all organs but lung, where exposure is very low for all nanoparticle types, and spleen, due to higher spleen exposure as discussed above. When comparing SH-Gel PEG Peptide to SH-Gel PEG, TE was also significantly higher for almost all organs. Exceptions were lung and kidney, where differences were not significant. The targeting effect of the added peptide is clearly illustrated by the above results, and more strikingly by the TE calculated for all organs pooled together, which was significantly almost twice higher for SH-Gel PEG Peptide when compared to SH-Gel NP (RTE = 1.783, $p = 0.0026$) and SH-Gel PEG ($p = 0.0051$), while SH-Gel PEG had similar global TE as SH-Gel NP (RTE = 0.965, $p = 0.8373$). These results confirm the high potency for SH-Gel PEG Peptide to target the tumor, and the benefits of adding the EGFR targeting peptide.

4. DISCUSSION

Several groups have shown that nanoparticles could serve as beneficial tumor targeting vehicles due to passive targeting strategy based on the enhanced permeability and retention (EPR) effect, whereby stealth shielding the particles with PEO/PEG surface modification prevent interaction with plasma protein, complement and uptake of reticuloendothelial system, improving circulation time of the nanoparticles.[4, 46, 47] Previous studies have shown that “enhanced permeation and retention” EPR effect is related to both particle size and

surface properties of nanoparticles. [4, 46-48] In a recent review paper of McNeil, the author has pointed out that nanoparticles with size (solid core) up to 220 nm could accumulate in tumors based on the EPR effect, especially for nanoparticles with negative zeta potential.[49] Modification with targeting moiety on surface of nanoparticles could achieve specific interaction with target cells as described in active targeting strategy.[41, 42]

Over-expression of EGFR receptors has been observed to correlate with poor prognosis in several types of cancers, including breast, ovarian, prostate, and pancreatic carcinomas.[50] The activating ligand such as EGF and the presence of other EGFR family co-receptors capable of forming heterodimers with EGFR govern the signaling output by the activated EGFR, leading to cell proliferation, differentiation, migration, adhesion, protection from apoptosis and transformation.[17, 51] Combined treatments with EGFR antibody (Erbitux®) and gemcitabine or taxanes (paclitaxel and docetaxel) was shown to significantly enhance therapeutic efficacy and decrease metastasis in preclinical and clinical studies.[21, 36] With EGFR receptor as targeting sites, the synthetic peptide GE11 can specifically bind to the receptors on the cell surface and induce cellular uptake of nanovectors without mitogenic activities, which prevents the activation of EGFR pathway.[30] Comparing this peptide with monoclonal antibody or even Fab fragment as targeting ligand, we could see that the size of the nanocarrier won't be changed significantly with peptide modification.

In the present study, we designed and prepared novel EGFR targeted thiolated gelatin nanoparticles as a delivery system for therapeutic agents in Panc-1 pancreatic carcinoma model. This system takes the advantage of disulfide crosslinks of thiolated gelatin to create a glutathione-responsive release system. PEG modification of thiolated gelatin nanoparticles could provide the hydrophilic shielding and achieve passive targeting to tumor site. Further conjugation with EGFR targeting peptide should assist the system in active targeting tumor cells with high expression of EGFR receptors. In our studies, the hydrodynamic diameter of SH-Gel PEG Peptide was around 230.8 ± 41.5 nm, and the zeta potential was −18.1 ± 4.02 mV, which shows that our particles fall into the categories of nanoparticles that could accumulate in tumors based on EPR effect. Meanwhile, for measurement of particle size, we were using dynamic light scattering technology to analyze the nanoparticles suspension, and the particle size could only reflect hydrodynamic particle size but not size of the solid core. Comparing to the scanning electron microscopy images, we could find out that the particle sizes in SEM were slightly smaller than the measurement results, which indicated that the sizes of solid core were smaller than the hydrodynamic particle sizes. This feature of nanoparticles could trigger the accumulation in the tumors based on mechanism of passive targeting.

To investigate the biodistribution and targeting characteristics of nanoparticles *in vivo*, we have used ICG encapsulated nanoparticles and 111In radiolabeled nanoparticles to qualitatively and quantitatively track drug and nanoparticles distribution over time in tumor. bearing SCID Beige mice *in vivo*.

The targeting effect of EGFR specific peptide was initially confirmed by our *in vivo* imaging studies, which indicated that ICG fluorescence signal in the tumor site was stronger than for the mice treated with SH-Gel PEG, SH-Gel NP and free ICG dye at 1 h. Although both SH-Gel PEG and SH-Gel PEG Peptide present a high level of signal, SH-Gel PEG Peptide induced sustainable exposure throughout the study till 12 h (Figure 2). All the nanoparticles systems present better delivery efficiency compared with free ICG dye, which was not detected in tumor site. The relatively lower *in vivo* fluorescence of the free dye is attributed to fluorescence quenching of free ICG in physiological environments[52-57] as well as aggregation and clearance from the body[53, 56]. As a lipophilic molecule, ICG is taken up exclusively by hepatic parenchymal cells and then secreted into the bile.[12] Clearance

process of ICG is consistent with our observations of hepatic localization and eventual clearance with acute renal involvement. With nanoparticles systems, it provides shielding effect, retarding emission loss during circulation, enabling greater fluorescence emission and extending circulation times for the encapsulated dye. Our results are consistent with a similar study of other polymeric *in vivo* delivery scheme.[58, 59] A comparison of signal intensity localized within the liver region at the 1 h time point shows a lower concentration of ICG nanoparticles undergoing hepatic uptake and bile secretion relative to the free dye control, further confirming that a greater concentration of ICG nanoparticles remains in circulation than free dye. As shown in Figure 2, longer retention time of nanoparticles systems permit the particles to passively or actively collect in the tumors region. Particles with sufficient circulation times will eventually extravasate and accumulate in solid tumors based on the enhanced permeability and retention (EPR) effect.[60-62] SH-Gel NP also showed tumor accumulation since 2 hours, but with significant lower signal intensity compared with the other two nanoparticles systems, and quick elimination at later time points. Although SH-Gel NP encapsulation of ICG is sufficient for *in vivo* shielding to provide prolonged fluorescence emission post systemic injection, the figure shows that SH-Gel PEG and SH-Gel PEG Peptide have sustained *in vivo* circulation that provides the tumor retention that is crucial for delivery of therapeutic agents.

Surprisingly, in quantitative biodistribution study with ^{111}Inlabeled nanoparticles, it appeared that PEG-modification decreased the blood MRT and terminal half-life of the nanoparticles. This result is not in line with most published results, reporting that PEG modification was associated with longer circulation time [63], although some other studies reported that PEG-modification did not enhance circulation time for some nanoparticle types[64, 65], or even increased it. A recent study also stated that, even conjugated with PEG, the majority of injected particles were eventually cleared from the blood by the reticuloendothelial system (RES) and the nanoparticles are accumulated in the liver and spleen.[66] Our results strongly suggest that PEG modification of the thiolated gelatin nanoparticles did not decrease opsonization process, contrarily to what is usually reported. With a decreased blood MRT, slightly higher liver concentrations and spleen concentrations significantly increased, it can be assumed that SH-Gel PEG and SH-Gel PEG Peptide nanoparticles are opsonized and cleared from the blood by circulating phagocytes and tissue macrophages (hepatic Kupffer cells and macrophages in the spleen) to a higher extent than SH-Gel NP nanoparticles-PEG modification results in the presence of a PEG corona on the nanoparticles, but also induces variations in other characteristics of the nanoparticles that could have an effect on PK, and account for the unusual MRT decrease. Moghimi states that the duration of particle circulation in the blood is both size and shape dependent.[67] He further suggests that nondeformable polymer-decorated spherical particles larger than 150 nm are highly prone to filtration at interendothelial cell slits of venous sinuses in the spleen, leading to targeting of the splenic red-pulp regions, which are highly rich in macrophages. Since PEG-modified nanoparticles displayed a size higher to this 150 nm limit (179.0 ± 30.9 nm and 230.8 ± 41.5 nm for SH-Gel PEG and SH-Gel PEG Peptide respectively), but not SH-Gel NP (132.6 ± 17.9 nm), this phenomenon could well account for the spleen higher concentrations and blood decreased MRT for PEG modified nanopartilces in our study. Accordingly, PEG modification did not significantly affect organ exposure except for spleen in which SH-Gel PEG and SH-Gel PEG Peptide accumulated more than SH-Gel NP, in line with other published results.[63, 68]

Despite the decreased MRT for PEG modified nanoparticles in the present study, the striking result is that blood MRT was high for all nanoparticle types, including SH-Gel NP (32.27 h). A very similar MRT of 33.64 h was also reported for gelatin nanoparticles by Saraogi.[68] Moreover, in the recently published study of Perry *et al.*[63], MRT calculated from their reported alpha and beta half-lives (HL alpha and HL beta) using the equation: MRT =

(HL alpha + HL beta)/0.693) were 22.6 h and 28.8 h for PEG Mushroom and PEG Brush respectively, in the same range as the MRT for SH-Gel PEG and SH-Gel PEG Peptide in our study (21.8 h and 15.3 h respectively). MRT in our study is calculated as $AUMC_{0\text{-}inf}$/ $AUC_{0\text{-}inf}$ by Phoenix® WinNonlin® and it is also related to CL and distribution volume by the following equation: V_{ss} = CL* MRT. In our study, the lower MRT for SH-Gel PEG and SH-Gel PEG Peptide versus SH-Gel NP cannot be associated to an increased clearance, since clearance is contrarily slightly, not significantly, lower for SH-Gel PEG and SH-Gel PEG Peptide (4.054 and 3.956 mL/h respectively) than for SH-Gel NP (5.376 mL/h). On the contrary, lower MRT might be predominantly related to a lower volume of distribution for SH-Gel PEG and SH-Gel PEG Peptide (88.2 mL and 60.6 mL respectively) than for SH-Gel NP (173.5mL). This higher V_{ss} for SH-Gel NP can well be linked to organ C_{last}/C_{max} data, as well as population analysis parameters, which show that SH-Gel NP will return with a smaller rate (K_{21}) from the peripheral organs where distributed, leading to higher accumulation in these organs. This higher distribution volume also explains the lower blood concentrations obtained after SH-Gel NP injection, even for the earliest time points. In line with our results, a lower volume of distribution has been reported for PEG modified nanoparticles[63], and particularly for PEG modified gelatin nanoparticles studied previous in our laboratory[46, 47]. The lower volume of distribution could be ascribed to less binding of PEG coated nanoparticles to non-specific tissue protein, as suggested by Jokerst *et al.*[69] These results underline the usefulness of the PEG-modification to reduce non-specific tissue distribution and enhance blood concentrations, according to the literature.[70]

Previous studies from our group with PEG modified gelatin or thiolated gelatin nanoparticles have shown similar half-life in the blood circulation systems (25.1h and 15.3h respectively)[46,47] comparing to 21.8 h in our study and also similar levels of distribution in other major organs. The major difference among these studies is the biodistribution of PEG modified nanoparticles into tumors. In both studies with breast tumor (MDA-MB-435)-bearing nude mice and subcutaneous pancreatic tumor-bearing SCID Beige mice, SH-Gel PEG showed much quick uptake into the tumors and sustainable accumulation throughout the whole study.[46] However, in the study with subcutaneous Lewis lung carcinoma (LLC) model in female C57BL/6J mice, slow accumulation of PEG modified gelatin nanoparticles in the tumor tissue were observed.[47] Kaul et al were using different PEG modification and radiolabelling process for synthesis of PEG modified gelatin nanoparticles.[47] Torchilin's group has also shown that the effective pore size of the blood vessels in LLC-bearing mice is significantly smaller than other tumor models.[71] As such, LLC-bearing mice model provided a challenge in formulation design that could be optimized based on the vascular permeability cut-off size.[47] Based on these, we could conclude that both the features of nanoparticles and levels of vasculatures in the tumors have critical impacts on the biodistribution of nanoparticles.

Despite wide distribution of nanoparticles in non-specific organs, previous studies with similar systems in tumor bearing mice have not shown any side effects. This might be due to the nature of nanoparticles systems.[47, 72-74] Gelatin polymers are derived from collagen, and have been used in food and medicines for long time. This type of polymers is biodegradable, non-toxic and non-immunogenic; with simply accumulation of these polymers in other organs, it would not trigger any severe side effects. After encapsulation of therapeutic reagents, toxicity studies with other organs are recommended with similar nanoparticular systems.

In our study, subcutaneous tumor model was established in SCID Beige mice for pharmacokinetic analysis of nanoparticles. Comparing the physiological features to human pancreatic ductal adenocarcinoma, the stroma surrounding might form additional barrier for delivery of therapeutic reagents. The stroma in Pancreatic ductal adenocarcinoma (PDAC) is

a complex structure, which consists of proliferating fibroblasts and pancreatic stella cells (PSCs). Activated pancreatic stella cells and fibroblasts usually present high level of various types of pro-fibrotic growth factor receptors, such as FGF, PDGF, IGF-1 or EGF.[75] With therapeutic reagents targeting on these receptors, it would suppress the proliferation of fibroblasts and PSCs. Interruption of stroma surrounding could eventually allow therapeutic agents to reach pancreatic cancer cells and complete their function.[75] This might help explain efficiency of different types of EGFR targeted therapeutics for cancer treatments including pancreatic cancer. Thus although the subcutaneous tumor model used in our PK study could not present all the features of pancreatic tumor environment, it could help interpret the targeting efficiency of our EGFR targeted therapy for *in vivo* model involving with overexpressed EGF receptor and demonstrate the potential therapeutic effects for treatment of cancers with high EGF receptor expression.

Addition of the peptide did not significantly modify blood pharmacokinetics when compared to SH-Gel PEG. The only significant pharmacokinetic difference between SH-Gel PEG and SH-Gel PEG Peptide actually occurred in the tumor tissue, where exposure (concentrations and AUC_{last}) was significantly higher when peptide was present. Moreover, the C_{last}/C_{max} ratio was higher, strongly suggesting that the SH-Gel PEG Peptide would be retained longer in the tumor tissue.

Overall, the addition of EGFR targeting peptide, in addition to PEG-modification, did not enhance blood MRT, which was already high for non-PEG modified nanoparticles. Contrarily, PEG-modification diminished non-specific tissue accumulation of the nanoparticles, which could decrease toxic risk and allow administration of higher doses of a therapeutic drug. Addition of the Peptide significantly increased the tumor targeting efficiency, which could help achieve the same therapeutic effect while administrating lower doses. Altogether, we can conclude that both targeting approaches are complimentary and SH-Gel PEG Peptide nanoparticles are a promising delivery system for anti-tumor drugs.

5. CONCLUSIONS

Thiolated type B gelatin nanoparticles have been successfully modified with the hydrophilic polymer PEG and EGFR targeting peptides, and the nanoparticles have size between150–250 nm. Qualitative biodistribution study with ICG encapsulated nanoparticles have shown nanoparticles are retained for prolonged periods of time in the tumor mass compared to free dye and EGFR targeted nanoparticles preferential accumulated in tumor especially at early time points. Quantitative biodistribution study has shown that radiolabeled nanoparticles present long circulation potential, and EGFR targeted nanoparticles showed preferential and sustainable accumulation in tumor sites compared to other nanoparticles. The resulting nanoparticulate systems with long circulation properties could be used to deliver therapeutic agents to solid tumors systemically based on passive and active targeting strategies by utilizing the enhanced permeability and retention effect of the tumor vasculature and specific interaction with cancer cell surface marker.

Acknowledgments

This study was supported by the National Cancer Institute's Alliance in Nanotechnology for Cancer's Center for Cancer Nanotechnology Excellence (CCNE) grant U54-CA151881. Scanning electron microscopy was performed at the Electron Microscopy Center of Northeastern University. Electron Spectroscopy for Chemical Analysis (ESCA) studies were performed at National ESCA and Surface Analysis Center for Biomedical Problems (NESAC/BIO), University of Washington, Seattle, WA. NESAC/BIO is supported by the NIH grant EB-002027.

7. REFERENCES

1. Xu J, Ganesh S, Amiji M. Non-condensing polymeric nanoparticles for targeted gene and siRNA delivery. Int J Pharm. 2012; 427(1):21–34. [PubMed: 21621597]
2. Choi SW, Lee SH, Mok H, Park TG. Multifunctional siRNA delivery system: polyelectrolyte complex micelles of six-arm PEG conjugate of siRNA and cell penetrating peptide with crosslinked fusogenic peptide. Biotechnol Prog. 2010; 26(1):57–63. [PubMed: 19918765]
3. Kim HK, Davaa E, Myung CS, Park JS. Enhanced siRNA delivery using cationic liposomes with new polyarginine-conjugated PEG-lipid. Int J Pharm. 2010; 392(1-2):141–7. [PubMed: 20347025]
4. van Vlerken LE, Duan Z, Little SR, Seiden MV, Amiji MM. Biodistribution and pharmacokinetic analysis of Paclitaxel and ceramide administered in multifunctional polymer-blend nanoparticles in drug resistant breast cancer model. Mol Pharm. 2008; 5(4):516–26. [PubMed: 18616278]
5. Kommareddy S, Tiwari SB, Amiji MM. Long-circulating polymeric nanovectors for tumor-selective gene delivery. Technol Cancer Res Treat. 2005; 4(6):615–25. [PubMed: 16292881]
6. Monsky WL, Fukumura D, Gohongi T, Ancukiewcz M, Weich HA, Torchilin VP, Yuan F, Jain RK. Augmentation of transvascular transport of macromolecules and nanoparticles in tumors using vascular endothelial growth factor. Cancer Res. 1999; 59(16):4129–35. [PubMed: 10463618]
7. Cho K, Wang X, Nie S, Chen ZG, Shin DM. Therapeutic nanoparticles for drug delivery in cancer. Clin Cancer Res. 2008; 14(5):1310–6. [PubMed: 18316549]
8. Matsumura Y, Maeda H. A new concept for macromolecular therapeutics in cancer chemotherapy: mechanism of tumoritropic accumulation of proteins and the antitumor agent smancs. Cancer Res. 1986; 46(12 Pt 1):6387–92. [PubMed: 2946403]
9. Napper, DH. Polymeric stabilization of colloidal dispersions. Academic Press; London ; New York: 1983. p. xvip. 428
10. Schafer FQ, Buettner GR. Redox environment of the cell as viewed through the redox state of the glutathione disulfide/glutathione couple. Free Radic Biol Med. 2001; 30(11):1191–212. [PubMed: 11368918]
11. Dong L, Xia S, Wu K, Huang Z, Chen H, Chen J, Zhang J. A pH/enzyme-responsive tumor-specific delivery system for doxorubicin. Biomaterials. 2010; 31(24):6309–16. [PubMed: 20472287]
12. Bulmus V, Woodward M, Lin L, Murthy N, Stayton P, Hoffman A. A new pH-responsive and glutathione-reactive, endosomal membrane-disruptive polymeric carrier for intracellular delivery of biomolecular drugs. J Control Release. 2003; 93(2):105–20. [PubMed: 14636717]
13. Garcea G, Neal CP, Pattenden CJ, Steward WP, Berry DP. Molecular prognostic markers in pancreatic cancer: a systematic review. Eur J Cancer. 2005; 41(15):2213–36. [PubMed: 16146690]
14. Wagner M, Greten FR, Weber CK, Koschnick S, Mattfeldt T, Deppert W, Kern H, Adler G, Schmid RM. A murine tumor progression model for pancreatic cancer recapitulating the genetic alterations of the human disease. Genes Dev. 2001; 15(3):286–93. [PubMed: 11159909]
15. Wagner M, Weber CK, Bressau F, Greten FR, Stagge V, Ebert M, Leach SD, Adler G, Schmid RM. Transgenic overexpression of amphiregulin induces a mitogenic response selectively in pancreatic duct cells. Gastroenterology. 2002; 122(7):1898–912. [PubMed: 12055597]
16. Leach SD. Mouse models of pancreatic cancer: the fur is finally flying! Cancer Cell. 2004; 5(1):7–11. [PubMed: 14749121]
17. Xiong HQ. Molecular targeting therapy for pancreatic cancer. Cancer Chemother Pharmacol. 2004; 54(Suppl 1):S69–77. [PubMed: 15316751]
18. Kimura K, Sawada T, Komatsu M, Inoue M, Muguruma K, Nishihara T, Yamashita Y, Yamada N, Ohira M, Hirakawa K. Antitumor effect of trastuzumab for pancreatic cancer with high HER-2 expression and enhancement of effect by combined therapy with gemcitabine. Clin Cancer Res. 2006; 12(16):4925–32. [PubMed: 16914581]
19. Safran H, Iannitti D, Ramanathan R, Schwartz JD, Steinhoff M, Nauman C, Hesketh P, Rathore R, Wolff R, Tantravahi U, Hughes TM, Maia C, Pasquariello T, Goldstein L, King T, Tsai JY, Kennedy T. Herceptin and gemcitabine for metastatic pancreatic cancers that overexpress HER-2/neu. Cancer Invest. 2004; 22(5):706–12. [PubMed: 15581051]

20. Yu D, Hung MC. Overexpression of ErbB2 in cancer and ErbB2-targeting strategies. Oncogene. 2000; 19(53):6115–21. [PubMed: 11156524]
21. Wilson CA, Cajulis EE, Green JL, Olsen TM, Chung YA, Damore MA, Dering J, Calzone FJ, Slamon DJ. HER-2 overexpression differentially alters transforming growth factor-beta responses in luminal versus mesenchymal human breast cancer cells. Breast Cancer Res. 2005; 7(6):R1058–79. [PubMed: 16457687]
22. Cheng J, Teply BA, Sherifi I, Sung J, Luther G, Gu FX, Levy-Nissenbaum E, Radovic-Moreno AF, Langer R, Farokhzad OC. Formulation of functionalized PLGA-PEG nanoparticles for in vivo targeted drug delivery. Biomaterials. 2007; 28(5):869–76. [PubMed: 17055572]
23. Song S, Liu D, Peng J, Sun Y, Li Z, Gu JR, Xu Y. Peptide ligand-mediated liposome distribution and targeting to EGFR expressing tumor in vivo. Int J Pharm. 2008; 363(1-2):155–61. [PubMed: 18692120]
24. Gu F, Zhang L, Teply BA, Mann N, Wang A, Radovic-Moreno AF, Langer R, Farokhzad OC. Precise engineering of targeted nanoparticles by using self-assembled biointegrated block copolymers. Proc Natl Acad Sci U S A. 2008; 105(7):2586–91. [PubMed: 18272481]
25. Townsend SA, Evrony GD, Gu FX, Schulz MP, Brown RH Jr. Langer R. Tetanus toxin C fragment-conjugated nanoparticles for targeted drug delivery to neurons. Biomaterials. 2007; 28(34):5176–84. [PubMed: 17854886]
26. Li Z, Zhao R, Wu X, Sun Y, Yao M, Li J, Xu Y, Gu J. Identification and characterization of a novel peptide ligand of epidermal growth factor receptor for targeted delivery of therapeutics. FASEB J. 2005; 19(14):1978–85. [PubMed: 16319141]
27. van Vlerken LE, Vyas TK, Amiji MM. Poly(ethylene glycol)-modified nanocarriers for tumor-targeted and intracellular delivery. Pharm Res. 2007; 24(8):1405–14. [PubMed: 17393074]
28. Vonhippel PH, Wong KY. Neutral Salts: The Generality of Their Effects on the Stability of Macromolecular Conformations. Science. 1964; 145(3632):577–80. [PubMed: 14163781]
29. Veis A. The physical chemistry of gelatin. Int Rev Connect Tissue Res. 1965; 3:113–200. [PubMed: 5318007]
30. Anand P, Kunnumakkara AB, Newman RA, Aggarwal BB. Bioavailability of curcumin: problems and promises. Mol Pharm. 2007; 4(6):807–18. [PubMed: 17999464]
31. Brandau DT, Jones LS, Wiethoff CM, Rexroad J, Middaugh CR. Thermal stability of vaccines. J Pharm Sci. 2003; 92(2):218–31. [PubMed: 12532371]
32. Hiraoka Y, Yamashiro H, Yasuda K, Kimura Y, Inamoto T, Tabata Y. In situ regeneration of adipose tissue in rat fat pad by combining a collagen scaffold with gelatin microspheres containing basic fibroblast growth factor. Tissue Eng. 2006; 12(6):1475–87. [PubMed: 16846345]
33. Abate-Shen C, Banach-Petrosky WA, Sun X, Economides KD, Desai N, Gregg JP, Borowsky AD, Cardiff RD, Shen M. M. Nkx3-1. Pten mutant mice develop invasive prostate adenocarcinoma and lymph node metastases. Cancer Res. 2003; 63(14):3886–90. [PubMed: 12873978]
34. Beaujeux R, Laurent A, Wassef M, Casasco A, Gobin YP, Aymard A, Rufenacht D, Merland JJ. Trisacryl gelatin microspheres for therapeutic embolization, II: preliminary clinical evaluation in tumors and arteriovenous malformations. AJNR Am J Neuroradiol. 1996; 17(3):541–8. [PubMed: 8881251]
35. Laurent A, Beaujeux R, Wassef M, Rufenacht D, Boschetti E, Merland JJ. Trisacryl gelatin microspheres for therapeutic embolization, I: development and in vitro evaluation. AJNR Am J Neuroradiol. 1996; 17(3):533–40. [PubMed: 8881250]
36. Soules MR, Dennis L, Bosarge A, Moore DE. The prevention of postoperative pelvic adhesions: an animal study comparing barrier methods with dextran 70. Am J Obstet Gynecol. 1982; 143(7): 829–34. [PubMed: 6179420]
37. Azarmi S, Huang Y, Chen H, McQuarrie S, Abrams D, Roa W, Finlay WH, Miller GG, Lobenberg R. Optimization of a two-step desolvation method for preparing gelatin nanoparticles and cell uptake studies in 143B osteosarcoma cancer cells. J Pharm Pharm Sci. 2006; 9(1):124–32. [PubMed: 16849014]
38. Mohanty B, Bohidar HB. Systematic of alcohol-induced simple coacervation in aqueous gelatin solutions. Biomacromolecules. 2003; 4(4):1080–6. [PubMed: 12857095]

39. Kommareddy S, Amiji M. Poly(ethylene glycol)-modified thiolated gelatin nanoparticles for glutathione-responsive intracellular DNA delivery. Nanomedicine. 2007; 3(1):32–42. [PubMed: 17379167]
40. Kommareddy S, Amiji M. Preparation and evaluation of thiol-modified gelatin nanoparticles for intracellular DNA delivery in response to glutathione. Bioconjug Chem. 2005; 16(6):1423–32. [PubMed: 16287238]
41. Xu J, Amiji M. Therapeutic gene delivery and transfection in human pancreatic cancer cells using epidermal growth factor receptor-targeted gelatin nanoparticles. J Vis Exp. 2012; (59):e3612. [PubMed: 22231028]
42. Magadala P, Amiji M. Epidermal growth factor receptor-targeted gelatin-based engineered nanocarriers for DNA delivery and transfection in human pancreatic cancer cells. AAPS J. 2008; 10(4):565–76. [PubMed: 19034673]
43. Kommareddy S, Amiji MM. Cell Transfection and Analysis Using DNA-Loaded Gelatin Nanoparticles. CSH Protoc. 2008; 2008 pdb prot4887.
44. Kommareddy S, Amiji MM. Intracellular trafficking studies using gold-encapsulated gelatin nanoparticles. CSH Protoc. 2008; 2008 pdb prot4886.
45. Kommareddy S, Amiji MM. Preparation and loading of gelatin nanoparticles. CSH Protoc. 2008; 2008 pdb prot4885.
46. Kommareddy S, Amiji M. Biodistribution and pharmacokinetic analysis of long. circulating thiolated gelatin nanoparticles following systemic administration in breast cancer-bearing mice. J Pharm Sci. 2007; 96(2):397–407. [PubMed: 17075865]
47. Kaul G, Amiji M. Biodistribution and targeting potential of poly(ethylene glycol)-modified gelatin nanoparticles in subcutaneous murine tumor model. J Drug Target. 2004; 12(9-10):585–91. [PubMed: 15621684]
48. Park K, Kim JH, Nam YS, Lee S, Nam HY, Kim K, Park JH, Kim IS, Choi K, Kim SY, Kwon IC. Effect of polymer molecular weight on the tumor targeting characteristics of self-assembled glycol chitosan nanoparticles. J Control Release. 2007; 122(3):305–14. [PubMed: 17643545]
49. McNeil SE. Nanoparticle therapeutics: a personal perspective. Wiley Interdiscip Rev Nanomed Nanobiotechnol. 2009; 1(3):264–71. [PubMed: 20049796]
50. Berz D, Miner T, McCormack E, Safran H. HER family inhibitors in pancreatic cancer: current status and future directions. Expert Opin Ther Targets. 2007; 11(3):337–47. [PubMed: 17298292]
51. Arteaga CL. The epidermal growth factor receptor: from mutant oncogene in nonhuman cancers to therapeutic target in human neoplasia. J Clin Oncol. 2001; 19(18 Suppl):32S–40S. [PubMed: 11560969]
52. Landsman ML, Kwant G, Mook GA, Zijlstra WG. Light-absorbing properties, stability, and spectral stabilization of indocyanine green. J Appl Physiol. 1976; 40(4):575–83. [PubMed: 776922]
53. Desmettre T, Devoisselle JM, Mordon S. Fluorescence properties and metabolic features of indocyanine green (ICG) as related to angiography. Surv Ophthalmol. 2000; 45(1):15–27. [PubMed: 10946079]
54. Simmons R, Shephard RJ. Does indocyanine green obey Beer's law? J Appl Physiol. 1971; 30(4): 502–7. [PubMed: 4929468]
55. Gathje J, Steuer RR, Nicholes KR. Stability studies on indocyanine green dye. J Appl Physiol. 1970; 29(2):181–5. [PubMed: 4913806]
56. Mordon S, Devoisselle JM, Soulie-Begu S, Desmettre T. Indocyanine green: physicochemical factors affecting its fluorescence in vivo. Microvasc Res. 1998; 55(2):146–52. [PubMed: 9521889]
57. Maarek JM, Holschneider DP, Harimoto J. Fluorescence of indocyanine green in blood: intensity dependence on concentration and stabilization with sodium polyaspartate. J Photochem Photobiol B. 2001; 65(2-3):157–64. [PubMed: 11809374]
58. Saxena V, Sadoqi M, Shao J. Polymeric nanoparticulate delivery system for Indocyanine green: biodistribution in healthy mice. Int J Pharm. 2006; 308(1-2):200–4. [PubMed: 16386861]
59. Altinoglu EI, Russin TJ, Kaiser JM, Barth BM, Eklund PC, Kester M, Adair JH. Near-infrared emitting fluorophore-doped calcium phosphate nanoparticles for in vivo imaging of human breast cancer. ACS Nano. 2008; 2(10):2075–84. [PubMed: 19206454]

60. Kong G, Braun RD, Dewhirst MW. Hyperthermia enables tumor-specific nanoparticle delivery: effect of particle size. Cancer Res. 2000; 60(16):4440–5. [PubMed: 10969790]
61. Maeda H. The enhanced permeability and retention (EPR) effect in tumor vasculature: the key role of tumor-selective macromolecular drug targeting. Adv Enzyme Regul. 2001; 41:189–207. [PubMed: 11384745]
62. Maeda H, Fang J, Inutsuka T, Kitamoto Y. Vascular permeability enhancement in solid tumor: various factors, mechanisms involved and its implications. Int Immunopharmacol. 2003; 3(3):319–28. [PubMed: 12639809]
63. Perry JL, Reuter KG, Kai MP, Herlihy KP, Jones SW, Luft JC, Napier M, Bear JE, DeSimone JM. PEGylated PRINT nanoparticles: the impact of PEG density on protein binding, macrophage association, biodistribution, and pharmacokinetics. Nano Lett. 2012; 12(10):5304–10. [PubMed: 22920324]
64. Li C, Wang C, Yang H, Zhao X, Wei N, Cui J. Liposomal topotecan formulation with a low polyethylene glycol grafting density: pharmacokinetics and antitumour activity. J Pharm Pharmacol. 2012; 64(3):372–82. [PubMed: 22309269]
65. Sun X, Rossin R, Turner JL, Becker ML, Joralemon MJ, Welch MJ, Wooley KL. An assessment of the effects of shell cross-linked nanoparticle size, core composition, and surface PEGylation on in vivo biodistribution. Biomacromolecules. 2005; 6(5):2541–54. [PubMed: 16153091]
66. Larson TA, Joshi PP, Sokolov K. Preventing protein adsorption and macrophage uptake of gold nanoparticles via a hydrophobic shield. ACS Nano. 2012; 6(10):9182–90. [PubMed: 23009596]
67. Moghimi SM, Hunter AC, Andresen TL. Factors controlling nanoparticle pharmacokinetics: an integrated analysis and perspective. Annu Rev Pharmacol Toxicol. 2012; 52:481–503. [PubMed: 22035254]
68. Saraogi GK, Gupta P, Gupta UD, Jain NK, Agrawal GP. Gelatin nanocarriers as potential vectors for effective management of tuberculosis. Int J Pharm. 2010; 385(1-2):143–9. [PubMed: 19819315]
69. Jokerst JV, Lobovkina T, Zare RN, Gambhir SS. Nanoparticle PEGylation for imaging and therapy. Nanomedicine (Lond). 2011; 6(4):715–28. [PubMed: 21718180]
70. Alexis F, Pridgen E, Molnar LK, Farokhzad OC. Factors affecting the clearance and biodistribution of polymeric nanoparticles. Mol Pharm. 2008; 5(4):505–15. [PubMed: 18672949]
71. Weissig V, Whiteman KR, Torchilin VP. Accumulation of protein-loaded long. circulating micelles and liposomes in subcutaneous Lewis lung carcinoma in mice. Pharm Res. 1998; 15(10): 1552–6. [PubMed: 9794497]
72. Kommareddy S, Amiji M. Antiangiogenic gene therapy with systemically administered sFlt-1 plasmid DNA in engineered gelatin-based nanovectors. Cancer Gene Ther. 2007; 14(5):488–98. [PubMed: 17363959]
73. Kaul G, Amiji M. Tumor-targeted gene delivery using poly(ethylene glycol)-modified gelatin nanoparticles: in vitro and in vivo studies. Pharm Res. 2005; 22(6):951–61. [PubMed: 15948039]
74. Bhavsar MD, Amiji MM. Gastrointestinal distribution and in vivo gene transfection studies with nanoparticles-in-microsphere oral system (NiMOS). J Control Release. 2007; 119(3):339–48. [PubMed: 17475358]
75. Korc M. Pancreatic cancer-associated stroma production. Am J Surg. 2007; 194(4 Suppl):S84–6. [PubMed: 17903452]

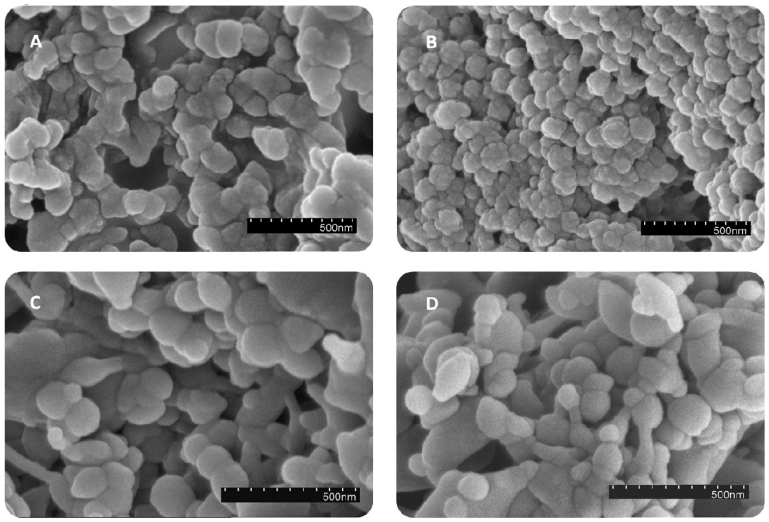

Figure 1.
Scanning electron microscopy images of (A) gelatin nanoparticles, (B) thiolated gelatin nanoparticles, (C) poly(ethylene glycol)-modified thiolated gelatin nanoparticles, and (D) EGFR targeted thiolated gelatin nanoparticles.

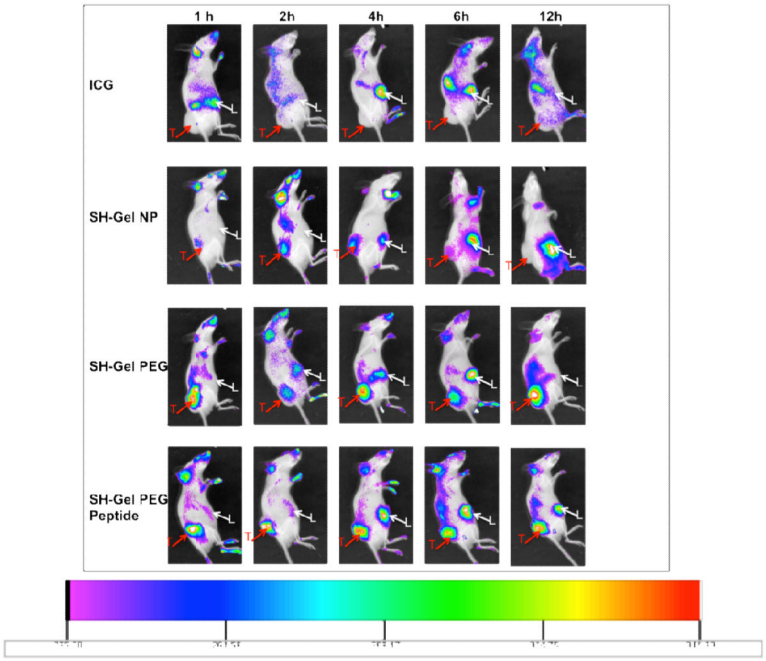

Figure 2.
Biodistribution of indocyanine green (ICG) near-IR dye encapsulated nanoparticles in mice for up to 12 hours (lateral view). ICG encapsulated thiolated gelatin (SH-Gel NP), poly(ethylene glycol)-modified (SH-Gel PEG) and EGFR targeted thiolated gelatin nanoparticles (SH-Gel PEG Peptide) were administered intravenously to female SCID beige mice bearing Panc-1 human pancreatic adenocarcinoma xenograft. (T=tumor; L=liver)

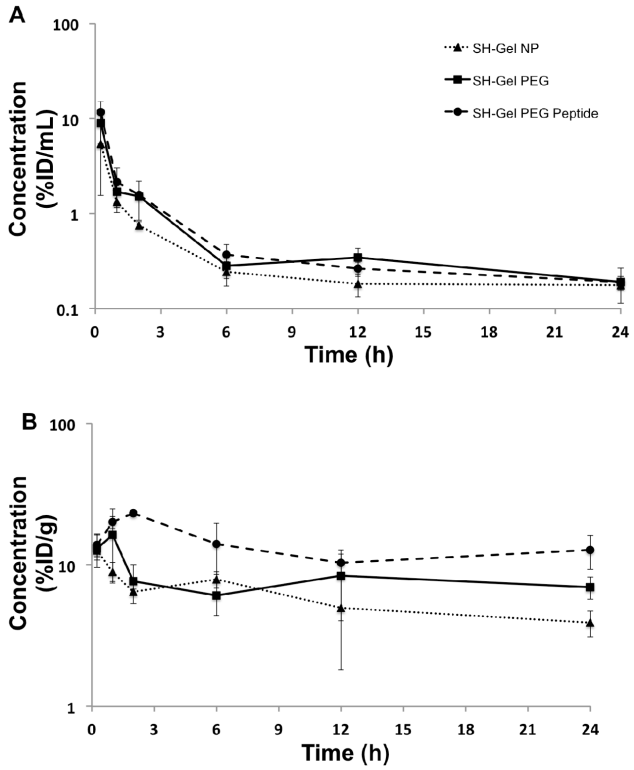

Figure 3.

Semi-logarithmic plot of nanoparticle concentrations in (A) Blood and (B) tumor as a function of time. ^{111}In labeled thiolated gelatin (SH-Gel NP), poly(ethylene glycol)-modified (SH-Gel PEG) and EGFR targeted thiolated gelatin nanoparticles (SH-Gel PEG Peptide) were administered intravenously to female SCID beige mice bearing Panc-1 human pancreatic adenocarcinoma xenograft. Results are presented as mean ± standard deviation (n=4). %ID = % injected dose.

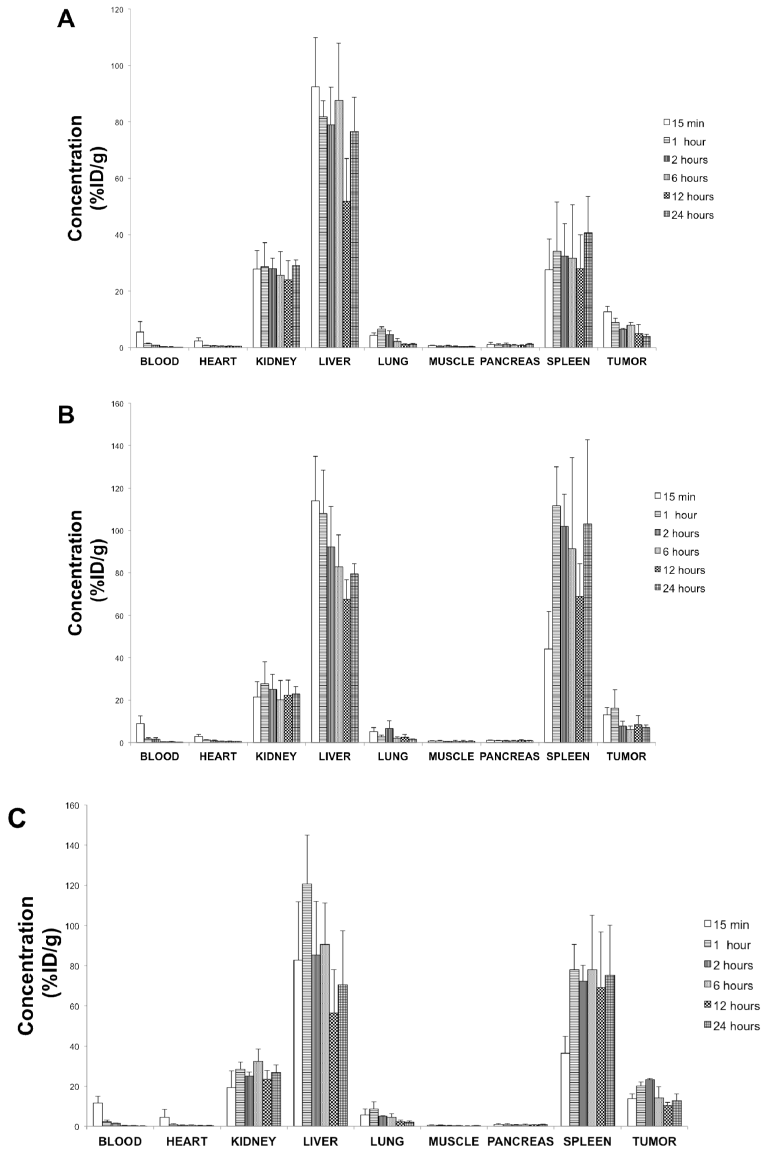

Figure 4.

Quantitative tissue biodistribution profile of ^{111}In labeled (A) thiolated gelatin (SH-Gel NP), (B) poly(ethylene glycol)-modified (SH-Gel PEG) and (C) EGFR targeted thiolated gelatin nanoparticles (SH-Gel PEG Peptide)at 15 min, 1, 2, 6, 12 and 24h after intravenous administration in Panc-1 tumor bearing mice. Results are presented as mean ± standard deviation (n=4). %ID = % injected dose.

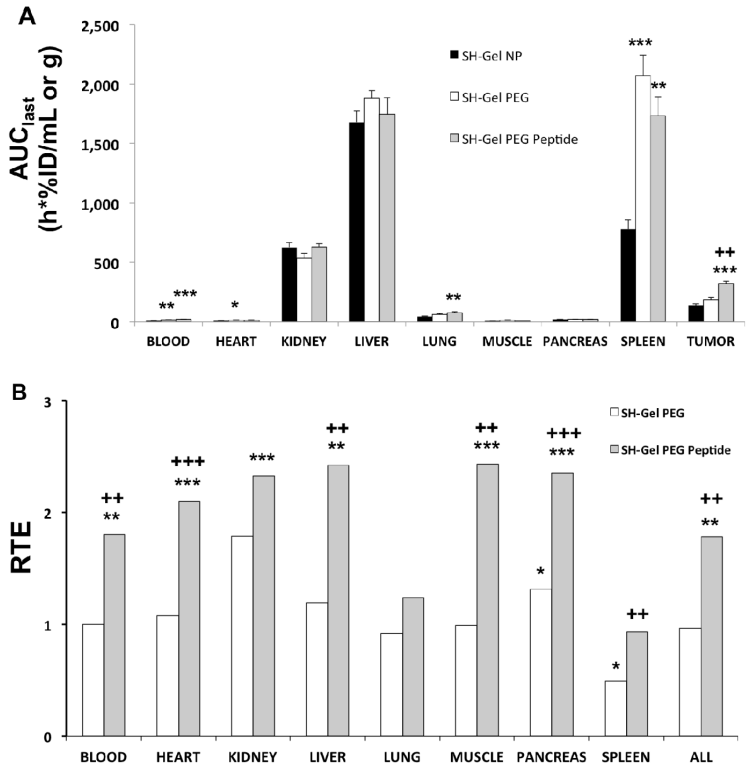

Figure 5.

Biodistribution in the organs and targeting efficiency. (A) Exposure of the main organs as evaluated by area under the concentration versus time curve from 0 to 24h (AUC_{last}) + standard error. (B) Relative targeting efficiency (RTE) of poly(ethylene glycol)-modified (SH-Gel PEG) and EGFR targeted thiolated gelatin nanoparticles (SH-Gel PEG Peptide) versus thiolated gelatin nanoparticles (SH-Gel NP). A value of 1 means similarity to SH-Gel NP targeting efficiency (TE). AUC_{last} and TE were compared between nanoparticle types using an unpaired t-test: * $p < 0.05$, ** $p < 0.01$, and *** $p < 0.001$ for comparison to SH-Gel NP; + $p < 0.05$, ++ $p < 0.01$, +++ $p < 0.001$ for comparison to SH-Gel PEG.

Table 1

Pharmacokinetic parameters evaluated by non-compartmental analysis (NCA) and population analysis (POP) of blood data using Phoenix® WinNonlin® software.

	NCA				POP		POP SE	
	SH-Gel NP	**SH-Gel PEG**	**SH-Gel PEG Peptide**		**SH-Gel NP**	**SH-Gel PEG ± Peptide**	**SH-Gel NP**	**SH-Gel PEG ± Peptide**
AUC_{inf} (h*%ID/mL)	**18.60**	**24.67**	**25.28**	**AUC_{inf} (h*%ID/mL)**	**20.74**		1.95	
CL (mL/h)	**5.376**	**4.054**	**3.956**	**CL (mL/h)**	**4.822**		0.454	
MRT (h)	**32.27**	**21.76**	**15.33**	**MRT (h)**	**31.19**	**19.47**	8.03	4.90
V_{ss} (mL)	**173.5**	**88.2**	**60.6**	**V_{ss} (mL)**	**150.4**	**93.9**	28.3	17.1
Lambda_z (1/h)	0.0224	0.0262	0.0332	Beta (1/h)	0.0198	0.0362	0.0042	0.0067
HL Lambda_z (h)	31.01	26.46	20.89	HL Beta (h)	35.05	19.16	7.53	3.57
AUC_{last} ± SE (h*%ID/mL)	10.71 (±1.01)	17.38 (±1.32)	19.56 (±1.01)	Alpha (1/h)	1.577	1.428	0.156	0.145
				HL Alpha (h)	0.4393	0.4852	0.0435	0.0494
				A (%ID/mL)	0.1270	0.1251	0.0140	0.0140
				B (%ID/mL)	0.002510	0.004333	0.000306	0.000516
				V_1 (mL)	7.724		0.835	
				V_2 (mL)	142.7	86.1	28.1	17.0
				K_e (1/h)	0.6242		0.0784	
				HL K_e (h)	1.110		0.139	
				K_{12} (1/h)	0.9231		0.1171	
				HL K_{12} (h)	0.7508		0.0952	
				K_{21} (1/h)	**0.04997**	**0.08276**	0.00803	0.01331
				HL K_{21} (h)	13.87	8.37	2.23	1.35

AUC = Area under the concentration versus time curve. AUC_{inf} = AUC until infinity. CL = Total body clearance. MRT = Mean Residence Time. V_{ss} = Steady State Volume of distribution. Lambda_z = Slope of the log-linear terminal phase (NCA). HL = Half life. AUC_{last} = AUC until last measurement time point. Beta = Slope of the log-linear terminal phase (POP). Alpha = Slope of the residual log-linear phase. A = Intercept of the residual log-linear phase. B = Intercept of the log-linear terminal phase. V_1 = Volume of the central compartment. V_2 = Volume of the peripheral compartment. K_e = Elimination rate constant from central compartment. K_{12} = Transfer rate constant from central compartment to peripheral compartment. K_{21} = Transfer rate constant from peripheral compartment to central compartment.

Table 2

C_{last}/C_{max} values in different organs. The highest value for each organ is colored in grey.

C_{last}/C_{max}	SH-Gel NP	SH-Gel PEG	SH-Gel PEG Peptide
Blood	0.0327	0.0213	0.0162
Heart	0.178	0.173	0.0972
Kidney	1.000	0.833	0.832
Liver	0.829	0.699	0.585
Lung	0.174	0.243	0.229
Muscle	0.468	0.805	0.525
Pancreas	1.000	0.841	0.956
Spleen	1.000	0.923	0.965
Tumor	0.309	0.428	0.550